Spectroscopic and Theoretical Studies of Oxygenated Dicopper(I) Complexes Containing Hydrocarbon-Linked Bis[2-(2-pyridyl)ethyl]amine Units: Investigation of a Butterfly $[Cu_2(\mu\text{-}\eta^2\text{:}\eta^2)(O_2)]^{2+}$ Core

Elna Pidcock,[†] Honorio V. Obias,[‡] Masaaki Abe,[‡] Hong-Chang Liang,[‡] Kenneth D. Karlin,*[,‡] and Edward I. Solomon*[,†]

Contribution from the Departments of Chemistry, Stanford University, Stanford, California 94305, and The Johns Hopkins University, Baltimore, Maryland 21218

Received September 15, 1998. Revised Manuscript Received November 17, 1998

Abstract: A series of side-on peroxide-bridged binuclear copper complexes $[Cu_2(NnPY2)(O_2)]^{2+}$ (where $n = 3-5$), which have been proposed to adopt a butterfly Cu_2O_2 geometry due to the constraints placed on the Cu−Cu distance by the alkyl chain linker of length $-(CH_2)_n-$, have been studied using absorption and resonance Raman spectroscopy and theoretical techniques. The four components of the peroxide to copper(II) charge-transfer transitions have been identified for the first time in the $[Cu_2(NnPY2)(O_2)]^{2+}$ (where $n = 3-5$) complexes. The observed shift of the peroxide O−O stretch by 25 cm^{-1} to higher energy and the changes observed in the energy and intensity of absorption bands including the presence of an additional band at 23 800−20 400 cm^{-1} (420−490 nm) (not seen in planar side-on peroxide-bridged dicopper cores) are correlated to the butterfly structure using transition dipole vector coupling and valence bond configuration interaction models. The identification of an absorption band at 23 800−20 400 cm^{-1} (420−490 nm) associated with the butterfly side-on peroxide-bridged dicopper core is important since the isomeric, bis(μ-oxo) core is also characterized by an absorption band in this region. The changes in bonding associated with a butterfly distortion of the Cu_2O_2 core are defined, and the reactivity of the butterfly core with respect to electrophilic aromatic substitution and H atom abstraction reactions is compared with that of the planar side-on peroxide-bridged dicopper core using the frontier molecular orbital description.

Introduction

The metalloprotein hemocyanin, responsible for O_2 transport, has been studied extensively.[1,2] The binuclear copper site binds dioxygen reversibly as peroxide, and a crystal structure obtained for the oxy form shows O_2^{2-} to be bound symmetrically in a side-on fashion, between two copper atoms 3.6 Å apart, forming a planar Cu_2O_2 core.[3] The absorption spectrum of oxyhemocyanin is characterized by an intense peroxide to copper(II) charge transfer (CT) transition at 345 nm ($\epsilon = 20\,000$ M^{-1} cm^{-1}), a weaker O_2^{2-}−Cu(II) CT transition at 570 nm ($\epsilon = 1000$ M^{-1} cm^{-1}) and a O_2^{2-} −Cu(II) CT feature in the CD spectrum at 485 nm.[1a] Some differences in the spectroscopy of oxyhemocyanins of different phyla exist, and these differences appear to correlate with differences observed in reactivity.[4] For example, the highest energy O_2^{2-}−Cu(II) CT transition shifts to higher energy and the splitting between the two lower energy O_2^{2-}−Cu(II) CT transitions increases on going from arthropod to mollusc hemocyanin; the small molecule binding constant is an order of magnitude less in arthropod hemocyanin, and the rate constant for displacement of peroxide from arthropod oxyhemocyanin is greater than for mollusc oxyhemocyanin by an order of magnitude. It has been suggested[4] that the differences in spectral properties and reactivity are caused by a distortion away from a planar Cu_2O_2 core of the active site.

After Karlin and co-workers suggested a side-on geometry as a possible binding mode for peroxide in earlier studies,[5,6] Kitajima et al.[7] structurally characterized the first $[Cu_2(\mu\text{-}\eta^2\text{:}\eta^2)(O_2)]^{2+}$ core in $[Cu(HB(3,5\text{-}i\text{-}Pr_2pz)_3)]_2^{2+}\cdot O_2$ (where HB(3,5-R_2pz)$_3$ is hydrotris(3,5-dialkyl-1-pyrazolyl)borate, R = ^{i}Pr). The Cu_2O_2 core was shown to be planar (Cu···Cu separation of 3.56 Å), and the absorption spectrum (R = ^{i}Pr, λ_{max} (ϵ, M^{-1} cm^{-1}) 350 nm (26 000) and 538 nm (2000)) is very similar to that of oxyhemocyanin. A resonance Raman spectrum showed a peak at 749 cm^{-1}, assigned as the peroxide O−O stretch.[8]

* To whom correspondence should be addressed. FAX: (650) 725-0259. E-mail: solomon@chem.stanford.edu.

[†] Stanford University.

[†] Johns Hopkins University.

(1) (a) Eickman, N. C.; Himmelwright, R. S.; Solomon, E. I. *Proc. Natl. Acad. Sci. U.S.A.* **1979**, *76*, 2094−2089. (b) Lowery, M. D.; Solomon, E. I. *Science* **1993**, *259*, 1575−1581. (c) Solomon, E. I.; Sundaram, U. M.; Machonkin, T. E. *Chem. Rev.* **1996**, *96*, 2563−2605. (d) Magnus, K. A.; Ton-That, H.; Carpenter, J. E. *Chem. Rev.* **1994**, *94*, 727−735.

(2) (a) Larrabee, J. A.; Spiro, T. G. *J. Am. Chem. Soc.* **1980**, *102*, 4217−4223. (b) Ling, J.; Nestor, L. P.; Czernuszewicz, R.; Spiro, T. G.; Fraczkiewicz, R.; Sharma, K. D.; Loehr, T. M.; Sanders-Loehr, J. *J. Am. Chem. Soc.* **1994**, *116*, 7682−7691.

(3) Magnus, K. A.; Hazes, B.; Ton-That, H.; Bonaventura, C.; Bonaventura, J.; Hol, W. G. J. *Proteins* **1994**, *19*, 302−309.

(4) Himmelwright, R. S.; Eickman, N. C.; Lubien, C. D.; Solomon, E. I. *J. Am. Chem. Soc.* **1980**, *102*, 5378−5388.

(5) Karlin, K. D.; Haka, M. S.; Cruse, R. W.; Meyer, C. J.; Farooq, A.; Gultneh, Y.; Hayes, J. C.; Zubieta, J. *J. Am. Chem. Soc.* **1988**, *110*, 1196−1207.

(6) Blackburn, N. J.; Strange, R. W.; Farooq, A.; Haka, M. S.; Karlin, K. D. *J. Am. Chem. Soc.* **1988**, *110*, 4263−4272.

(7) Kitajima, N.; Fujisawa, K.; Moro-oka, Y.; Toriumi, K. *J. Am. Chem. Soc.* **1989**, *111*, 8975−8976.

10.1021/ja983310e CCC: $18.00
Published on Web 02/03/1999

Chart 1

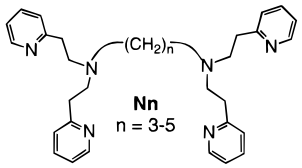

Chart 2

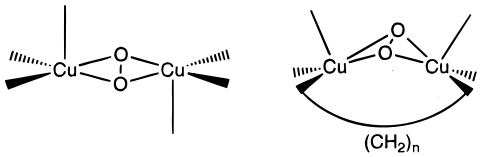

A novel Cu_2O_2 core has been structurally characterized by Tolman[9,10] and Stack.[11] The cores, formulated as $[Cu^{III}_2(\mu\text{-}O)_2]^{2+}$, have spectral features distinct from those associated with side-on-bridged binuclear copper peroxo cores; the absorption spectrum of $[(TACN^{Bn3})_2Cu_2(\mu\text{-}O)_2]^{2+}$ (where $TACN^{R3}$ is a N,N′,N″-trisubstituted 1,4,7-triazacyclononane) exhibits bands at 318 nm (ϵ = 12 000 M^{-1} cm^{-1}) and 430 nm (ϵ = 14 000 M^{-1} cm^{-1}),[9] and the resonance Raman spectrum is characterized by a very intense peak at ~600 cm^{-1}, which is assigned as the symmetric Cu−O core stretch.

A series of compounds $[Cu_2(NnPY2)(O_2)]^{2+}$ (where N*n*PY2 are binucleating ligands with two bis[2-(2-pyridyl)ethyl]amine tridentate ligands (PY2), linked via the amino nitrogen by $-(CH_2)_n-$ groups (n = 3−5)) (Chart 1) have been prepared and characterized.[12]

Extended X-ray absorption fine structure (EXAFS) data have been collected on $[Cu_2(N4PY2)(O_2)]^{2+}$ and $[Cu_2(N3PY2)O_2]^{2+}$.[6] The Cu···Cu separation for $[Cu_2(N4PY2)(O_2)]^{2+}$ was determined to be 3.4 Å, and the Cu···Cu separation for $[Cu_2(N3PY2)(O_2)]^{2+}$ was found to be even shorter at 3.2 Å (cf. $[Cu(HB(3,5\text{-}R_2pz)_3)]^{2+}\cdot O_2$; the Cu···Cu separation is 3.56 Å). These results led to the proposal that as the methylene chain linker was shortened (N4 to N3) the Cu_2O_2 core "butterflys" to accommodate the shorter Cu···Cu separation (Chart 2).

The absorption spectra of $[Cu_2(NnPY2)(O_2)]^{2+}$ (n = 3−5) (henceforth referred to as N3, N4, and N5, respectively) all show an intense band at ~360 nm (ϵ = 15 000−21 400 M^{-1} cm^{-1} depending on n), a weak CT at ~550 nm, and an additional band at 420−490 nm, not seen in the absorption spectra of $[Cu(HB(3,5\text{-}R_2pz)_3)]_2(O_2)$. A related series of complexes, where the tridentate PY2 units are linked by a xylyl group, also show an absorption band at ~430 nm in addition to absorption features at 360 and 530 nm, upon oxygenation of the Cu(I) precursor.[13] An interesting possibility was that the additional band (relative to the side-on bridged structure) derives from the bis(μ-oxo) core. However, using resonance Raman spectroscopy, it was established that the absorption band at 430 nm was associated with the $[Cu_2(\mu\text{-}\eta^2\text{:}\eta^2)(O_2)]^{2+}$ core and was not due to a mixture of $[Cu_2(\mu\text{-}\eta^2\text{:}\eta^2)(O_2)]^{2+}$ and $[Cu_2(\mu\text{-}O)_2]^{2+}$ species.[14]

The unusual charge-transfer spectra obtained for $[Cu_2(NnPY2)(O_2)]^{2+}$ (where n = 3−5), associated with an out-of-plane distortion of the $\mu\text{-}\eta^2\text{:}\eta^2$ peroxide, indicate that there are large changes in the electronic structure of the butterfly core compared with that of the planar side-on peroxide-bridged structure. We use absorption and resonance Raman spectroscopy and density functional theory (DFT) to define these changes and examine how the electronic description of the butterfly core relates to the electronic structure of other peroxide binding modes to copper and to reactivity.

Experimental Section

The $[Cu_2(NnPY2)(O_2)][A^-]_2\cdot CH_3CN$ (where A^- is $[ClO_4]^-$ for N3, $[PF_6]^-$ or $[BArF]^-$ for N4, and $[PF_6]^-$ for N5) precursors for solution samples were prepared as reported previously.[12,15] The absorption spectra of $[Cu_2(NnPY2)O_2][ClO_4\text{-}]_2$ (where n = 3−5) were obtained at −80 °C in CH_2Cl_2 by using the HP 8452 diode array spectrophotometer with OLIS diode-array Operating System Version 15.01 program. The spectrophotometer was adapted with a light-proof rectangular box fitted to the sample compartment to allow the insertion of a Kontes KM-611772 variable-temperature vis/UV Dewar cell (including cuvette assembly). Cooling was achieved by inserting a coil of copper tubing into the methanol-filled Dewar through which cold methanol was circulated from an external source (Neslab ULT-95DD Cryocool immersion cooler, with Endocal refrigerated circulating pump). The temperature was monitored with an Omega Model 651 resistance thermometer probe. Resonance Raman spectra were obtained using a Princeton Instruments ST-135 back-illuminated CCD detector on a Spex 1877 CP triple monochromator with 1200, 1800, and 2400 grooves/mm holographic spectrograph gratings. The excitation was provided by Coherent I90C-K Kr^+ and Innova Sabre 25/7 Ar^+ CW ion lasers. A polarization scrambler was used between the sample and the spectrometer. Spectral resolution was <2 cm^{-1}. Samples for solution Raman spectra were prepared by dissolving substituted $[Cu^I_2(NnPY2)][A^-]_2.1CH_3CN$ in CH_2Cl_2 or CH_3COCH_3 in an NMR tube and oxygenating at −80 °C. The sample tube was spun with an air-driven NMR spinner and cooled to ~180 K by a N_2-flow system. Integrated peak intensities used to determine resonance Raman profiles were measured relative to the 700 cm^{-1} peak of CH_2Cl_2 or to the 790 cm^{-1} peak of CH_3COCH_3 for solution samples. Isotopic substitution was achieved by oxygenation of the complex with $^{18}O_2$ (Isotech, 99% labeled).

Electronic structure calculations using the 1982 QCPE version of the SCF-Xα-SW package[16] were run on IBM 3BT-RS/6000 computers. The exchange values α used in the atomic spheres are those of Schwarz.[17] The inner- and outer-sphere α values were the valence-electron weighted averages of the atomic α values. Norman sphere radii were used for all atoms except copper. A copper sphere radius of 2.95 bohr is used (Norman radius = 2.35 bohrs), as this radius has been found to better reproduce the ground- and excited-state spectral features

(8) Baldwin, M. J.; Root, D. E.; Pate, J. E.; Fujisawa, K.; Kitajima, N.; Solomon, E. I. *J. Am. Chem. Soc.* **1992**, *114*, 10421−10431.

(9) Halfen, J. A.; Mahapatra, S.; Wilkinson, E. C.; Kaderli, S.; Young, V. G.; Que, L.; Zuberbühler, A. D.; Tolman, W. B. *Science* **1996**, *271*, 1397−1400.

(10) Mahapatra, S.; Halfen, J. A.; Wilkinson, E. C.; Pan, G.; Wang, X.; Young, V. G.; Cramer, C. J.; Que, L.; Tolman, W. B. *J. Am. Chem. Soc.* **1996**, *118*, 11555−11574.

(11) Mahadavan, V.; Hou, Z. G.; Cole, A. P.; Root, D. E.; Lal, T. K.; Solomon, E. I.; Stack, T. D. P. *J. Am. Chem. Soc.* **1997**, *119*, 11996−11997.

(12) Karlin, K. D.; Tyeklár, Z.; Farooq, A.; Haka, M. S.; Ghosh, P.; Cruse, R. W.; Gultneh, Y.; Hayes, J. C.; Toscano, P. J.; Zubieta, J. *Inorg. Chem.* **1992**, *31*, 1436−1451.

(13) Karlin, K. D.; Nasir, M. S.; Cohen, B. I.; Cruse, R. W.; Kaderli, S.; Zuberbühler, A. D. *J. Am. Chem. Soc.* **1994**, *116*, 1324−1336.

(14) Pidcock, E.; Obias, H. V.; Xin Zhang, C.; Karlin, K. D.; Solomon, E. I. *J. Am. Chem. Soc.* **1998**, *120*, 7841−7847.

(15) Karlin, K. D.; Haka, M. S.; Cruse, R. W.; Meyer, G. J.; Farooq, A.; Gultneh, Y.; Hayes, J. C.; Zubieta, J. *J. Am. Chem. Soc.* **1988**, *110*, 1196−1207.

(16) (a) Johnson, K. H.; Norman, J. G., Jr.; Connolly, J. W. D. *Computational Methods for Large Molecules and Localized States in Solids*; Plenum: New York, 1973. (b) Slater, J. C. *The Self-Consistent Field for Molecules and Solids: Quantum Theory of Molecules and Solids*; McGraw-Hill: New York, 1974; Vol 4. (c) Connolly, J. W. D. *Semiempirical Methods of Electronic Structure Calculation*; Plenum: New York, 1977; Part A (Techniques). (d) Cook, M. R., Ph.D. Thesis, Harvard University, 1981. (e) Case, D. A. *Annu. Rev. Phys. Chem.* **1982**, *33*, 151−171. (f) Cook, M. R.; Case, D. A. *QCPE Program #465*, **1982**, *33*, 21−22.

(17) Schwarz, K. *Phys. Rev. B* **1972**, *5*, 2466−2468.

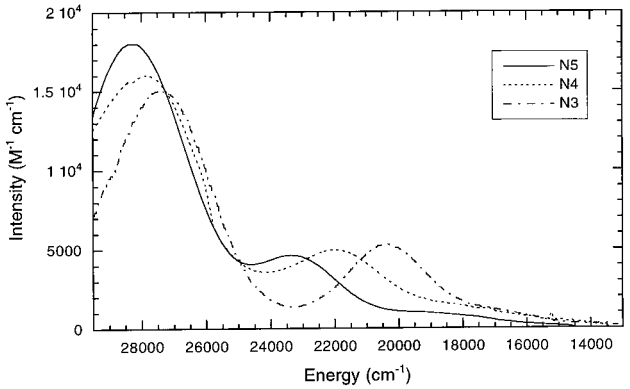

Figure 1. UV−visible absorption spectra obtained for $[Cu_2(NnPY2)O_2][ClO_4]_2$ (where $n = 3-5$) in CH_2Cl_2 at −80 °C.

in $CuCl_4^{2-}$ and plastocyanin.[18,19] A Watson sphere with a radius equal to that of the outer sphere and charge equal but opposite to that of the model was included for ionic models. Calculations were considered to be converged when the maximum relative change in the atomic potential between successive iterations was less than 10^{-5} Rydbergs. The coordinates used for the spin-restricted and spin-unrestricted SCF-Xα-SW calculations on the planar and butterfly $[(NH_3)_4Cu_2(O_2)]^{2+}$ cores are given in the Supporting Information.

Spectra were fitted to Gaussian band shapes using a modified Levenburg−Marquardt constrained nonlinear least-squares fitting routine.

Results

The electronic absorption spectra obtained for $[Cu^{II}(N5PY2)(O_2)][PF_6]_2$, $[Cu^{II}(N4PY2)(O_2)][PF_6]_2$, and $[Cu^{II}(N3PY2)(O_2)][PF_6]_2$ show an intense feature at approximately 27 800 cm^{-1} (360 nm) which decreases in intensity upon shortening the alkyl chain (ϵ (M^{-1} cm^{-1}) = 21 400 (N5), 16 000 (N4), 15 000 (N3)), a less intense feature which shifts to lower energy (23 600 cm^{-1} (423 nm) for N5, 21 800 cm^{-1} (458 nm) for N4, and 20 400 cm^{-1} (490 nm) for N3) and gains intensity (ϵ (M^{-1} cm^{-1}) 3600 (N5), 4500 (N4), 5300 (N3)), and a weak feature which also shifts to lower energy (19 200 cm^{-1}, 520 nm (N5); 18 200 cm^{-1}, 550 nm (N4); 16 700 cm^{-1}, 600 nm (N3); ϵ 1200 M^{-1} cm^{-1}) as the Cu···Cu distance decreases.[12] Spectra of $[Cu^{II}(NnPY2)(O_2)][ClO_4]_2$ (where $n = 3-5$) are shown in Figure 1. These spectra are qualitatively similar to that of $[Cu(HB(3,5\text{-}i\text{-}Pr_2pz)_3]_2(O_2)$,[6] with the exception of the additional absorption band in the 23 800−20 400 cm^{-1} region and the decrease in intensity of the highest energy O_2^{2-}−Cu(II) CT band at ∼27 800 cm^{-1}.

Resonance Raman spectra, obtained using an excitation wavelength of 458 nm, of N4 oxygenated with $^{16}O_2$ and $^{18}O_2$ are shown in Figure 2. The resonance Raman peak at 750 cm^{-1}, which shifts with $^{18}O_2$ substitution to 709 cm^{-1}, is assigned to the O−O stretch of a side-on-bound peroxide on the basis of its frequency and isotope shift (41 cm^{-1}). Raman peaks at 297 and 596 cm^{-1}, which show no $^{18}O_2$ dependency, are also observed. The peak at 297 cm^{-1} is assigned to the symmetric Cu−O stretch of a μ-η^2:η^2 core which primarily involves motion of the coppers and hence shows no isotope shift.[6] The peak at 596 cm^{-1} (∼2 × 297 cm^{-1}) is assigned to the overtone of the symmetric core stretch on the basis of its frequency and lack of isotope effect. The peak at 1050 cm^{-1} (which shifts 50 cm^{-1} upon $^{18}O_2$ substitution) is assigned as the overtone of the asymmetric (and hence unobserved) Cu−O stretch at ∼525 cm^{-1}.[6] Resonance Raman spectra with $^{16}O_2$ and $^{18}O_2$ have also been obtained for N3 and N5. The oxygenated complexes of N3 and N5 exhibit the symmetric Cu−Cu core stretch at 293 and 281 cm^{-1}, respectively, which show no isotope shift and weak stretches assigned to the overtone of the symmetric core stretch at 585 and 560 cm^{-1}, respectively. The resonance Raman peak assigned as the symmetric O−O stretch is observed at 764 cm^{-1} in N3 and 741 cm^{-1} in N5 (cf. N4 ν_{O-O} 750 cm^{-1}; Figure 3). Therefore, the O−O stretch moves to higher energy as the alkyl chain linker gets shorter, and the Cu···Cu separation lessens.

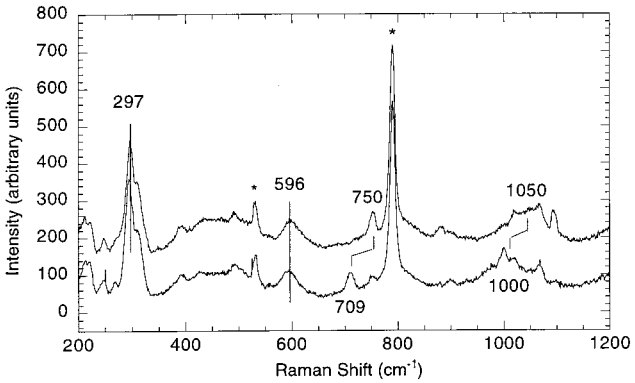

Figure 2. Resonance Raman spectra obtained for solutions of $^{16}O_2$ and $^{18}O_2$ $[Cu_2(N4PY2)O_2]^{2+}$ in acetone (excitation wavelength 458 nm). Peaks sensitive to oxygen isotope substitution are labeled with their Raman shifts; an asterisk denotes peaks derived from acetone solvent.

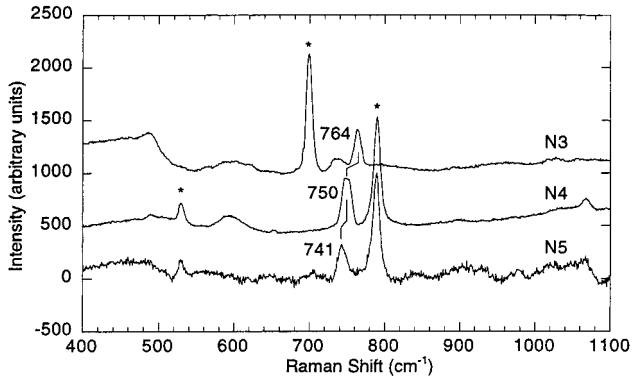

Figure 3. Resonance Raman spectra obtained for solutions of $[Cu_2(N3PY2)O_2]^{2+}$ in dichloromethane (excitation wavelength 458 nm), $[Cu_2(N4PY2)O_2]^{2+}$ in acetone (excitation wavelength 407 nm), and $[Cu_2(N5PY2)O_2]^{2+}$ in acetone (excitation wavelength 413 nm). An asterisk denotes peaks derived from solvent.

To probe the origin of the absorption band at 23 800−20 400 cm^{-1} observed in the N*n* series (Figure 1), resonance Raman spectra were recorded using excitation wavelengths nearly coincident with the λ_{max} of this band for N5, N4, and N3 (Figure 4). The resonance Raman spectra show peaks consistent with oxygen bound as peroxide in a side-on bridging geometry, but no intense stretch at ∼600 cm^{-1}, which would be characteristic of the symmetric Cu−O core stretch of a bis(μ-oxo) isomer, is observed.[10,11] The resonance Raman spectra show enhancement of the symmetric Cu−Cu core stretch at 270−300 cm^{-1}, indicating that the additional absorption band must be assigned as a O_2^{2-}−Cu(II) charge-transfer transition associated with the side-on peroxide-bound Cu_2O_2 core.

Resonance Raman profiles obtained for the Cu−O stretch and the peroxide O−O stretch for a solution of $N4[BArF]_2$ in acetone are shown in Figure 5. The symmetric Cu−Cu core stretch at 297 cm^{-1} gains enhancement from the absorption

(18) Gewirth, A. A.; Cohen, S. L.; Schugar, H.; Solomon, E. I. *Inorg. Chem.* **1987**, *26*, 1133−1146.
(19) Gewirth, A. A.; Solomon, E. I. *J. Am. Chem. Soc.* **1988**, *110*, 3811−3819.

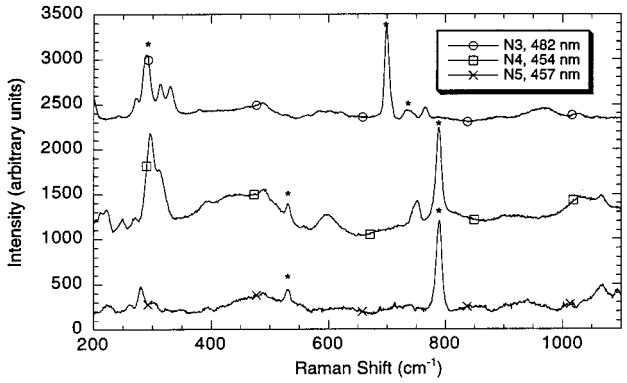

Figure 4. Resonance Raman spectra obtained for solutions of $[Cu_2(N3PY2)O_2]^{2+}$ in dichloromethane (excitation wavelength 482 nm), $[Cu_2(N4PY2)O_2]^{2+}$ in acetone (excitation wavelength 454 nm), and $[Cu_2(N5PY2)O_2]^{2+}$ in acetone (excitation wavelength 458 nm). An asterisk denotes peaks derived from solvent.

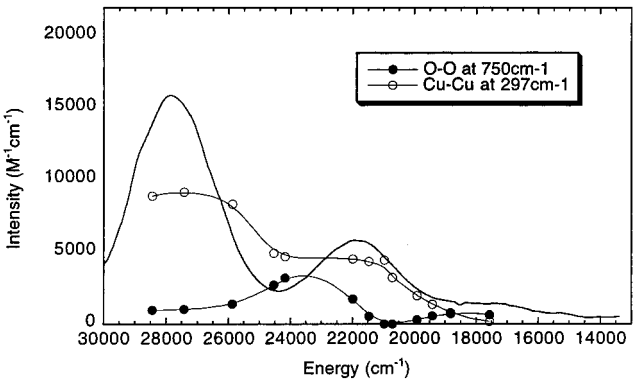

Figure 5. Resonance enhancement profiles of 297 cm^{-1} (●) and 750 cm^{-1} (○) Raman peaks vs the absorption spectrum of $[Cu_2(N4PY2)O_2]^{2+}$ in dichloromethane solution.

bands at 27 800 cm^{-1} (360 nm) and 21 800 cm^{-1} (458 nm), and the O−O stretch has maxima in the enhancement profile at approximately 23 500 cm^{-1} (425 nm) and 18 300 cm^{-1} (550 nm). The profiles obtained for N5 and N3 are qualitatively similar (Supporting Information) with the Cu−Cu stretch (at 280−295 cm^{-1}) enhanced by the absorption bands at 27 800 cm^{-1} (360 nm) and 22 600 cm^{-1} (423 nm) for N5 and 27 400 cm^{-1} (365 nm) and 20 400 cm^{-1} (490 nm) for N3, and the profiles of the O−O stretch exhibit two maxima, one coincident with the lowest energy O_2^{2-}−Cu(II) CT band and the other at approximately 24 600 cm^{-1} (407 nm) for N5 and 22 700 cm^{-1} (440 nm) for N3, in the region between the two resolved, higher energy CT bands.

Analysis

Spectral Assignments. When peroxide binds to a single copper(II) ion, the peroxide π^* orbitals split into two nondegenerate levels, π^*_σ and π^*_v. The π^*_σ orbital is situated in the Cu−O−O plane and has a strong σ-donor interaction with the Cu $d_{x^2-y^2}$ orbital; therefore, the π^*_σ−Cu $d_{x^2-y^2}$ CT band is at high energy is and intense, due to good overlap between the donor and acceptor orbitals. The π^*_v orbital is oriented vertically to the Cu−O−O plane (Chart 3) and has a weak π interaction with the out-of-plane Cu d orbitals but not Cu $d_{x^2-y^2}$; the π^*_v−Cu $d_{x^2-y^2}$ CT band is thus at low energy and is weak due to the poor overlap between the donor and acceptor orbitals.[20] The

(20) Solomon, E. I.; Tuczek, F.; Root, D. E.; Brown, C. A. *Chem. Rev.* **1994**, *94*, 827−856.

Chart 3

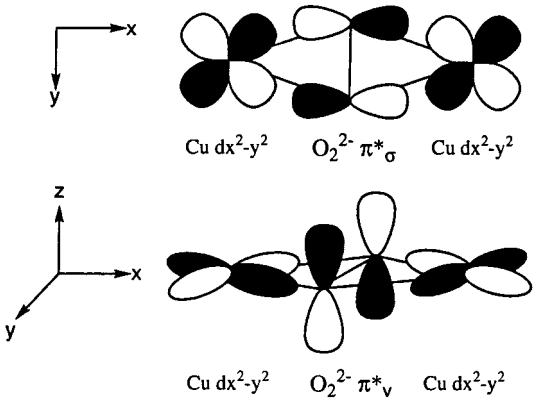

equivalent in-plane (π^*_σ) and out-of-plane (π^*_v) peroxide orbitals of the Cu_2O_2 core are shown in Chart 3.

Using a localized, valence bond description, each monomer O_2^{2-}−Cu(II) CT transition is further split in a dimer into two components, which are the symmetric and antisymmetric combinations of the CT transitions to each of the two Cu $d_{x^2-y^2}$ orbitals. The absorption spectrum of the binuclear copper side-on bridged peroxide dimer model $[Cu(HB(3,5\text{-}i\text{-}Pr_2pz)_2]_2(O_2)$ has bands at 350 nm (ϵ (M^{-1} cm^{-1}) = 26 000) and 538 nm (ϵ = 2000) assigned as the peroxide π^*_σ−Cu(II) and the π^*_v−Cu(II) charge-transfer transitions, respectively.[6] In the approximate C_{2h} symmetry of the planar core (*trans*-axial N donor ligands), transitions involving a single component of the π^*_σ and π^*_v levels are electric dipole allowed; hence, only two bands are observed in the absorption spectrum. The resonance Raman profile of the low-energy Cu−Cu core stretch at 277 cm^{-1} shows enhancement from the π^*_σ to Cu(II) CT transition, and the peroxide O−O stretch at 755 cm^{-1} is enhanced by the π^*_v to Cu(II) CT and, to a lesser degree, by the π^*_σ−Cu(II) CT transition.

In the approximate C_{2v} dimer symmetry of the tethered binuclear Cu_2O_2 cores of the N*n* series (where the *x* direction is parallel to the Cu−Cu vector and the *y* direction is parallel to the O−O vector), the peroxide π^*_σ and π^*_v orbitals transform as A_2 and B_2, respectively, and the positive and negative combinations of the copper $d_{x^2-y^2}$ orbitals from molecular orbitals have A_2 and B_2 symmetry; therefore, the two components of both the π^*_σ and π^*_v CT transitions have $A_1(z)$ and $B_1(x)$ symmetry. Thus, *all four O_2^{2-} to Cu(II) CT transitions are electric dipole allowed*. The profiles obtained for N5, N4, and N3 of the low-energy symmetric Cu−O core stretch show enhancement not only from the absorption band at ∼27 800 cm^{-1} (360 nm), analogous to the case for $[Cu(HB(3,5\text{-}i\text{-}Pr_2pz)_3]_2(O_2)$, but also from the absorption band in the region of 23 800−20 400 cm^{-1} (423−490 nm) (depending on the length of the alkyl chain). Thus, these absorption bands are assigned as the two components of the π^*_σ−Cu(II) CT transition. The profiles of the peroxide O−O stretch for N5, N4, and N3 all show enhancement from the low-energy CT band at 19 200−16 700 cm^{-1} (520−600 nm), and it is therefore assigned as one component of the π^*_v−Cu(II) CT transition. The profiles also exhibit maxima in the energy region between the two π^*_σ−Cu(II) CT bands, indicating that the second component of the π^*_v−Cu(II) CT transition is present at approximately 25 000−22 200 cm^{-1} (400−450 nm) but is obscured by the more intense π^*_σ bands to higher and lower energy. The resonance Raman profiles of the O−O stretch for the N*n* series show very little enhancement from the highest energy π^*_σ−Cu(II) CT transition. This indicates that there is negligible interference (i.e. resonance

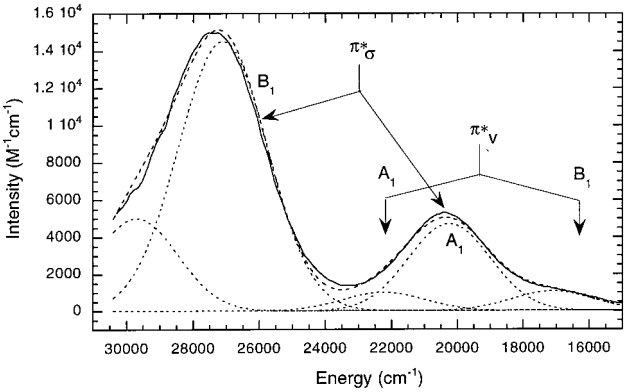

Figure 6. Absorption spectrum (solid line) and fits obtained using Gaussian analysis (dashed lines) for $[Cu_2(N3PY2)O_2]^{2+}$. An additional band centered at 29 700 cm^{-1} (HWHM = 1800 cm^{-1}) assigned to a N_{PY2}−Cu(II) CT transition[32] was used to fit the high-energy region of the absorption spectrum.

de-enhancement)[21] between the two excited states, and therefore, the energy at which the profile of the O−O stretch peaks will be roughly coincident with the energy at which the intensity of the peroxide π^*_v−Cu(II) CT transition maximizes.

Therefore, from the resonance Raman profiles it appears that all four components of the O_2^{2-} π^*_σ and π^*_v CT transitions (two A_1 and two B_1) are present and the additional band in the absorption spectrum (at 23 800−20 400 cm^{-1}) is assigned to the second component of the π^*_σ−Cu(II) CT transition, which gains significant intensity upon bending the Cu_2O_2 core. Good fits to the absorption spectra were achieved using a Gaussian analysis including four bands. The absorption spectrum and Gaussian fit obtained for N3 are shown in Figure 6, and the fit parameters obtained for N3, N4, and N5 are given in Table 1. The band maxima of the higher energy component of the π^*_v−Cu(II) CT transition in N3, N4, and N5 are found to be at 22 230, 26 300, and 24 700 cm^{-1}, respectively, nearly coincident with the maxima in the resonance Raman profiles of the peroxide O−O stretch obtained for N3, N4, and N5 at 22 700, 23 500, and 24 600 cm^{-1}.

The intensities of the two components of the π^*_σ−Cu(II) CT transitions appear to be correlated with the length of the alkyl chain linker; as the copper−copper separation decreases (N5 to N3), the high-energy π^*_σ transition loses intensity and the lower energy π^*_σ−Cu(II) CT gains intensity (4600 M^{-1} cm^{-1} in N5 to 5200 M^{-1} cm^{-1} for N3 (Figure 1)). Using a transition dipole vector coupling (TDVC) model[1a] the intensity ratio between the two components of a LMCT transition is given by

$$I_{A1}/I_{B1} = (\vec{M}_1 + \vec{M}_2)^2/(\vec{M}_1 - \vec{M}_2)^2 = \sin^2(\Phi/2)/\cos^2(\Phi/2) \quad (1)$$

where $\vec{M}_1$ and $\vec{M}_2$ are transition dipoles from the center of the O−O bond to each of the Cu atoms, the positive combination of $\vec{M}_1$ and $\vec{M}_2$ corresponds to the A_1 CT transition and the negative combination to the B_1 CT transition, and Φ is the angle between the two Cu−O−O planes.

From Chart 4, bending the Cu_2O_2 plane and hence decreasing Φ from 180° (planar) to ∼130° (in N3) leads to a decrease in the intensity of the B_1 component (when $\Phi = 180°$, $\sin^2(\Phi/2) = 1$) and an increase in the intensity of the A_1 component (since when $\Phi = 180°$, $\cos^2(\Phi/2) = 0$). Thus, the effect on intensity of bending the Cu_2O_2 plane as modeled by TDVC is qualitatively in agreement with the spectral changes observed on going from N5 to N3; the highest energy component of the π^*_σ−Cu(II) CT loses intensity and is assigned as the B_1 transition and the lower energy component gains intensity and is assigned as the A_1 transition (Table 1).

Electronic Structure Calculations. The resonance Raman spectra of N5, N4, and N3 indicate that the strength of the O−O bond increases as the Cu···Cu distance shortens (ν_{O-O}(N5 to N3) 741−765 cm^{-1}), and the electronic absorption spectra for the N*n* series indicate there are significant perturbations in the electronic structure relative to that of the planar side-on peroxide-bridged binuclear copper core. SCF-Xα-SW density functional calculations[16] were performed on $[(NH_3)_4Cu_2(O_2)]^{2+}$ cores in planar[22] and butterfly geometries to allow for a comparison of the electronic structures of the cores and to probe the effects of bending the Cu_2O_2 plane on peroxide O−O and Cu−O interactions.[23] In both the planar and butterfly cores, the Cu−O distance is 1.9 Å and the O−O distance is 1.4 Å. The planar core has a Cu···Cu separation of 3.6 Å, and the angle between the Cu−O−O planes is 180°; the butterfly core is described by a Cu···Cu separation of 3.2 Å and an angle between the Cu−O−O planes of 130°. A comparison of the contributions from peroxide and Cu d orbitals to a key subset of molecular orbitals and their energies for the planar and butterfly structures are given in Table 2 and shown in the energy level diagram in Figure 7.

Electronic Structure Description. The electronic absorption spectra of the N*n* series show a decrease of 15% in the total intensity of the π^*_σ−Cu(II) CT transitions upon bending the Cu_2O_2 plane (Table 1); therefore, the overlap between the Cu $d_{x^2-y^2}$ orbital and the peroxide π^*_σ orbital is poorer in the butterfly core. In accord with this observation, in the butterfly structure, the orbital comprising a large percentage of peroxide π^*_σ ($4a_2$) has moved to lower binding energy (when compared with the equivalent orbital in the planar core, $3b_{2g}$), indicating that, as the Cu_2O_2 core is bent, the bonding interaction between the in-plane π^*_σ and $d_{x^2-y^2}$ orbitals is lessened, and the π^*_σ containing molecular orbital is less stabilized. Reciprocally, the LUMO, which is the antibonding combination of the π^*_σ and $d_{x^2-y^2}$ orbitals in both the planar and butterfly structures (Figure 8, top), is less destabilized in the butterfly core compared to the planar core (Figure 7) and the energy separation between the π^*_σ and the LUMO has decreased. In addition, bending the Cu_2O_2 plane allows a significant interaction between the negative combination of the Cu $d_{x^2-y^2}$ orbitals and the π^*_v orbital, resulting in a shift of the π^*_v-containing MO, relative to that of the side-on peroxide core to approximately 2 eV deeper binding energy (cf. $3b_{1g}$ and $6b_2$; Figure 7). The HOMO of the butterfly core involves an antibonding interaction between the negative combination of the Cu $d_{x^2-y^2}$ orbitals and the peroxide π^*_v orbital (Figure 8, bottom); this molecular orbital is destabilized relative to the planar structure due to the increased interaction between the Cu $d_{x^2-y^2}$ and the peroxide π^*_v orbitals (Figure 7, $5b_{3u}$ and $8b_2$). In addition, the stabilizing contribution to the HOMO from the peroxide π acceptor, σ^* orbital, in the planar structure (Figure 8, bottom left) has decreased upon bending (from 1.7% to 0.5%), further destabilizing the HOMO

(21) (a) Stein, P.; Miskowski, V.; Woodruff, W. H.; Griffith, J. P.; Werner, K. G.; Gaber, B. P.; Spiro, T. G. *J. Chem. Phys.* **1976**, *64*, 2159−2167. (b) Shin, K. S. K.; Zink, J. I. *J. Am. Chem. Soc.* **1990**, *112*, 7148−7157. (c) Meyers, A. B. *Chem. Rev.* **1996**, *96*, 911−926.

(22) Ross, P. K.; Solomon, E. I. *J. Am. Chem. Soc.* **1991**, *113*, 3246−3259.

(23) The Amsterdam density functional program gives results in accord with those obtained from SCF-Xα-SW, performed with an adjusted sphere radius of 2.95 bohr. SCF-Xα calculations were used, to to be compatible with the calculations performed previously on the planar $[(NH_3)_4Cu_2O_2]^{2+}$ core.[22]

Table 1. Parameters Obtained for Gaussian Fits of Absorption Spectra of $[Cu_2(NnPY_2)O_2][ClO_4]_2$ (Where $n = 3-5$) in CH_2Cl_2

component of peroxide to Cu(II) CT	$[Cu_2(N3PY2)(O_2)]^{2+}$ energy (HWHM) (cm^{-1})	intensity (M^{-1} cm^{-1})	oscillator strength (f)	$[Cu_2(N4PY2)(O_2)]^{2+a}$ energy (HWHM) (cm^{-1})	intensity (M^{-1} cm^{-1})	oscillator strength (f)	$[Cu_2(N5PY2)(O_2)]^{2+}$ energy (HWHM) (cm^{-1})	intensity (M^{-1} cm^{-1})	oscillator strength (f)
B_1 π^*_σ	27 100 (1 900)	14 500	0.127	27 850 (2 200)	15 900	0.161	28 025 (2 000)	17 500	0.161
A_1 π^*_v	22 230 (1 750)	1 000	0.008	23 600 (2 100)	1 000	0.010	24 700 (1 800)	950	0.008
A_1 π^*_σ	20 240 (1 750)	4 700	0.038	21 800 (2 100)	4 450	0.043	23 100 (1 800)	3 975	0.033
B_1 π^*_v	17 100 (1 750)	1 050	0.008	17 850 (2 100)	1 000	0.010	19 400 (1 800)	900	0.007

[a] Absorption bands consistently broader in spectrum obtained for $[Cu_2(N4PY2)(O_2)][ClO_4]_2$.

Chart 4

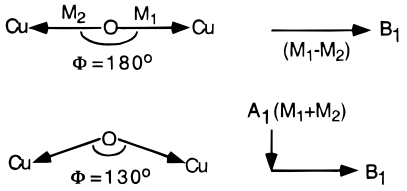

Table 2. Energy Levels and Charge Distribution for Planar and Butterfly $[(NH_3)_4Cu_2O_2]^{2+}$ Cores

planar $[(NH_3)_4Cu_2(O_2)]^{2+}$ core level	energy (eV)	charge distribn (%) Cu	O	N	butterfly $[(NH_3)_4Cu_2(O_2)]^{2+}$ core level	energy (eV)	charge distribn (%) Cu	O	N
$5b_{2g}$ LUMO	−5.38	67	15	17	$7a_2$ LUMO	−4.32	68	15	16
$5b_{3u}$ HOMO	−6.49	73	3	23	$8b_2$ HOMO	−4.77	64	20	16
$3b_{1g}$ π^*_v	−6.89	21	79	0	$6b_2$ π^*_v	−7.63	49	46	4
$2b_{2u}$ π^b_v	−11.73	24	76	0	$4a_2$ π^*_σ	−10.38	51	40	8
$3b_{2g}$ π^*_σ	−12.02	49	48	2	$6a_1$ π^b_v	−11.56	23	76	1
$4a_g$ σ^b	−13.63	7	92	1	$5a_1$ σ^b	−12.76	9	90	0
$2b_{1u}$ π^b_σ	−17.45	46	54	0	$2b_1$ π^b_σ	−15.20	44	56	0

of the butterfly core (Figure 7). The combined effects of the LUMO being less destabilized and the HOMO being more destabilized in the butterfly core with respect to the planar core accounts for the calculated decrease in the HOMO−LUMO splitting of 0.6 eV upon bending the Cu_2O_2 plane.

Bonding Considerations. To determine the origin of a stronger peroxide O−O bond observed with resonance Raman spectroscopy and to establish the nature of Cu−O bonding interactions in the butterfly core, a comparison of the occupancies of the bonding and antibonding peroxide orbitals and a selection of the Cu orbitals between the planar and butterfly cores has been made and the results are given in Table 3. The largest changes observed in the populations of the peroxide orbitals between the two core geometries are seen in the peroxide π^b_σ, π^b_v, and π^*_v orbitals. The peroxide π^b_σ orbital has symmetry-allowed interactions with the negative combination of the Cu d_{xy} orbitals and Cu $4p_x$ orbitals. The negative combination of the Cu d_{xy} orbitals is fully occupied, and therefore charge donation from the peroxide π^b_σ orbital can occur to only the unoccupied Cu $4p_x$ orbitals. As can be seen in Table 3, the occupancy of the Cu $4p_x$ orbital decreases and the occupancy of the peroxide π^b_σ orbital increases, indicating a reduced interaction between these orbitals as the oxygens are lifted out of the plane. An increased occupancy of the π^b_σ orbital increases the O−O bond strength. The occupancies of the peroxide π^b_v and π^*_v orbitals decrease upon bending the Cu_2O_2 core; however, the loss of charge is greater from the π^*_v orbital. As stated earlier, the peroxide π^*_v orbitals have an increased

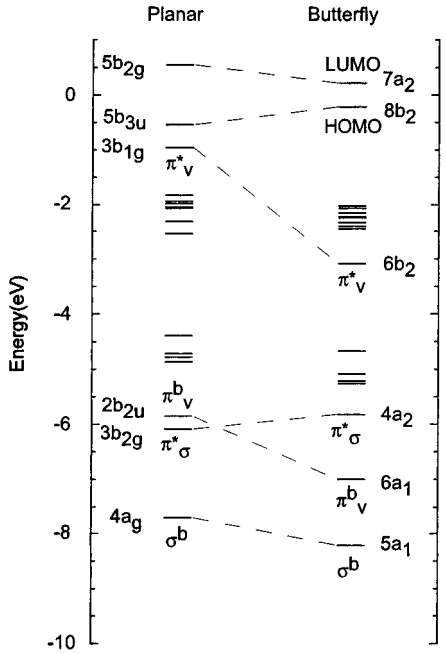

Figure 7. Energy level diagram calculated for a $[(NH_3)_4Cu_2O_2]^{2+}$ core in a planar (D_{2h}) (right) and a butterfly (C_{2v}) (left) geometry. The energy scale has been linearly shifted such that 0 eV is centered between the energies of the HOMO and LUMO for both geometries.

interaction with the negative combination of the Cu $d_{x^2-y^2}$ orbitals, resulting in a stabilized π^*_v MO and a destablized HOMO. However, since the negative combination of the Cu $d_{x^2-y^2}$ orbital is fully occupied, these interactions do not represent an increase in charge donation from the peroxide π^*_v orbital to the Cu d orbitals and hence a decrease in occupancy of the peroxide π^*_v orbital. In the butterfly core there is a symmetry-allowed interaction between the π^*_v orbitals and the positive combination of the Cu $4p_y$ orbitals, not present in the planar core. The total occupancy of the π^*_v orbital decreases by 0.06 electron and the occupancy of the positive combination of the Cu $4p_y$ orbital in the π^*_v molecular orbital increases by a similar amount (0.09 electron). Therefore, the decreased occupancy of the peroxide π^*_v orbital is due to charge donation into the unoccupied Cu $4p_y$ orbital. The absorption spectra of the N*n* series do not show a significant increase in the intensity of the $\pi^*_v \rightarrow$Cu(II) CT transitions (Table 1), in accord with the results from the calculations which show charge donation is into a orbital at much higher energy.

Bending the plane has little effect upon the populations of the σ^* and σ^b atomic orbitals, which therefore do not contribute to the strengthening or weakening of the O−O bond. Thus, the back-bonding into the σ^* orbital present in the planar structure

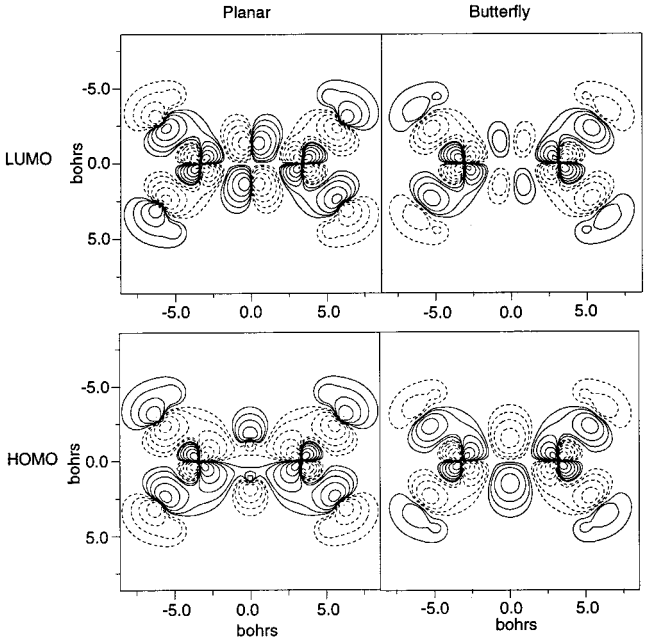

Figure 8. Contour plots of coefficients of the electron density of the LUMO (top) and HOMO (bottom) for a $[(NH_3)_4Cu_2O_2]^{2+}$ core in a planar (D_{2h}) (left) and a butterfly (C_{2v}) (right) geometry from spin-unrestricted Xα calculations. Contours are taken in the *xy* plane (*x* direction along Cu−Cu axis, *y* direction along O−O bond). The contour of the HOMO of the butterfly structure (bottom, right) shows the cross-section of the lower lobes of the peroxide π^*_v orbital.

Table 3. Electron Populations, Determined from Xα Calculations, for Planar and Butterfly $[(NH_3)_4Cu_2O_2]^{2+}$ Cores

atomic orbital	electron occ for the planar $[(NH_3)_4Cu_2(O_2)]^{2+}$ core	electron occ for the butterfly $[(NH_3)_4Cu_2(O_2)]^{2+}$ core	Δe^-
Cu $4p_x$	0.58	0.51	−0.07
Cu $4p_y$	0.46	0.47	+0.01
Cu $4p_z$	0.11	0.14	+0.03
π^*_σ	0.59	0.59	0.00
π^*_v	0.91	0.85	−0.06
σ^*	0.06	0.06	0.00
π^b_σ	0.54	0.57	+0.03
π^b_v	0.83	0.79	−0.04
σ^b	0.95	0.95	0.00

does not change in the butterfly core. The reduced interaction between the π_σ orbitals and the Cu $4p_x$ orbitals leads to an increase in the occupancy of the π^b_σ orbital, which leads to a stronger O−O bond. A result of the increased interaction between the peroxide π_v orbitals and Cu d and π orbitals is a decrease in the population of the π_v orbitals; π^*_v decreases in occupancy more than π^b_v, due to charge donation into the unoccupied Cu $4p_y$ orbital, again increasing the O−O bond strength. The resonance Raman spectra of N5, N4, and N3 show the O−O peak shifts to higher energy (∼25 cm^{-1}) as the methylene chain shortens, in accord with the molecular orbital description of the change in bonding of a butterfly core.

The slightly decreased interaction between the π^b_σ and π^*_σ orbitals and the unoccupied Cu 3d and Cu 4p orbitals would be expected to weaken the Cu−O bonding. However, in the butterfly core, a new interaction between the Cu $4p_y$ and the peroxide π^*_v orbitals (forbidden in the planar geometry) will be stablilizing with respect to Cu−O bonding. Therefore, the net Cu−O bonding interactions are reasonably similar between the planar and the butterfly cores.

Valence Bond Configuration Interaction (VBCI): Analysis of CT Transition Energies. The changes in intensity of the

Table 4. VBCI Parameters (cm^{-1}) Derived from Xα Calculations and Results from VBCI Calculations for Planar and Butterfly $[(NH_3)_4Cu_2O_2]^{2+}$ Cores

	planar, C_{2h}[a] (cm^{-1})	butterfly, C_{2v} (cm^{-1})
Δ_σ	54 430	42 790
Δ_v	7 740	22 960
$(h_{d\tau})_\sigma$	−23 050	−13 090
$(h_{d\tau})_v$	−6 600	−9 640
MMCT	52 430	52 430
DCT	140 000	119 200
π^*_σ	$\Delta E[^1B_u{}^{CT}-{}^1A_g{}^{GS}] = 44\,330$	$\Delta E[^1B_1{}^{CT}-{}^1A_1{}^{GS}] = 43\,160$
	$\Delta E[^1A_g{}^{CT}-{}^1A_g{}^{GS}] = 46\,260$	$\Delta E[^1A_1{}^{CT}-{}^1A_1{}^{GS}] = 42\,290$
π^*_v	$\Delta E[^1B_u{}^{CT}-{}^1A_g{}^{GS}] = 19\,520$	$\Delta E[^1B_1{}^{CT}-{}^1A_1{}^{GS}] = 26\,844$
	$\Delta E[^1A_g{}^{CT}-{}^1A_g{}^{GS}] = 22\,410$	$\Delta E[^1A_1{}^{CT}-{}^1A_1{}^{GS}] = 31\,110$

[a] From ref 24

A_1 and B_1 components of the π^*_σ −Cu(II) CT transitions exhibited by N5, N4, and N3 have been described by applying the TDVC model to a butterfly Cu_2O_2 core (see Spectral Assignments). Coupled with the changes in intensity are changes in the energies of the A_1 and B_1 components of both the π^*_σ −Cu(II) and π^*_v −Cu(II) transitions (vide supra). A VBCI model has been developed to describe the energy splittings of LMCT transitions in binuclear complexes which includes configuration interaction with the ground state and other higher energy charge transfer states.[24,25] For a dimeric Cu(II) complex bridged in a μ-η^2:η^2 fashion by peroxide, the highest energy orbitals of peroxide, π^*_σ and π^*_v, and the highest energy, singly occupied $d_{x^2-y^2}$ orbitals of the two copper centers are included in the model. In the ground state it is assumed that each unpaired electron is primarily localized on one copper center, hence, the valence bond formalism. A ligand-to-metal charge-transfer transition corresponds to the transfer of one electron from a peroxide orbital (π^*_σ or π^*_v) to the $d_{x^2-y^2}$ orbital on each copper. Thus, both the π^*_σ−Cu(II) and π^*_v−Cu(II) states are doubly degenerate in the dimer and are described by the symmetric and antisymmetric combinations of the CT transitions to each copper of the dimer. The VBCI model describes the loss of this degeneracy by allowing the ground state, metal-to-metal charge-transfer configuration (MMCT, where one electron is transferred from one copper to the other) and the double charge-transfer configuration (DCT, where the two electrons of the peroxide π^*_σ orbital are transferred, one to each copper of the dimer) to interact with the two components of the π^*_σ and π^*_v CT states. Secular determinants describe the configuration interaction (CI) of the ligand to metal CT states with the ground state and higher lying CT states (vide infra). Overlap of the metal and ligand orbitals allows for this CI and is taken into account by the transfer matrix element $(h_{d\tau})_i$ (i = v, σ).

Previously, excited LMCT state splittings of oxyhemocyanin have been calculated.[24] The MO ground and CT triplet $M_s = 1$ state wave functions are identical with those of the valence bond description.[24,25] The active site of oxyhemocyanin was modeled using a simplified $[(NH_3)_4Cu_2(O_2)]^{2+}$ planar core (D_{2h}), and the relative energies of the MO triplet states were determined with SCF-Xα-SW transition state calculations (vide infra). These energies were related to the VBCI parameters—the zeroth-order energies for the π^*_σCT (Δ_σ), π^*_vCT (Δ_v), and DCT as well as the magnitude of the transfer matrix element $(h_{d\tau})_\sigma$ (Table 4). The zeroth-order energy for the MMCT state was assumed to be equal to the Mott−Hubbard energy U, from photoelectron spectroscopy. In D_{2h} symmetry the π^*_v orbital has no overlap with the copper $d_{x^2-y^2}$ orbitals, and hence $(h_{d\tau})_v$

(24) Tuczek, F.; Solomon, E. I. *J. Am. Chem. Soc.* **1994**, *116*, 6916−6924.
(25) Tuczek, F.; Solomon, E. I. *Inorg. Chem.* **1993**, *32*, 2850−2862.

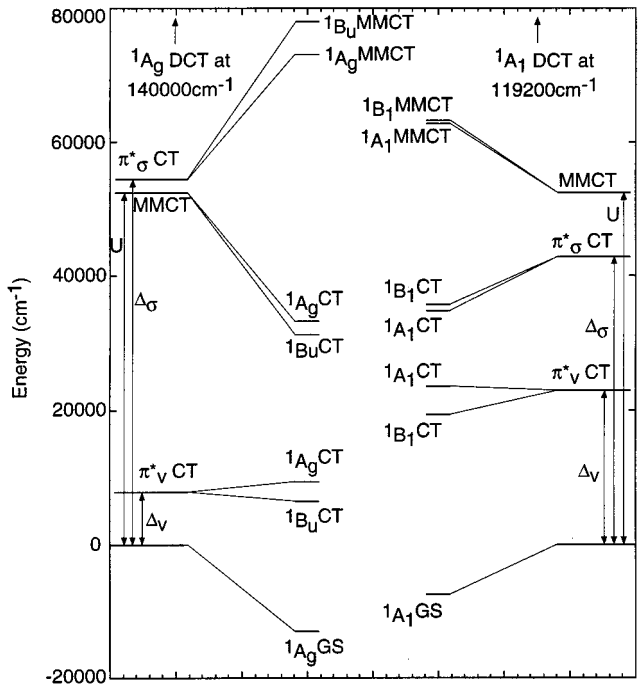

Figure 9. VBCI diagram for a side-on peroxide-bridged copper dimer in planar (left) and butterfly (right) geometries. Unperturbed singlet states are shown for both planar and butterfly geometries (far left and far right, respectively) and after CI is introduced between the GS, CT, and higher energy CT states (MMCT and DCT, DCT omitted from diagram for clarity) (center left, planar; center right, butterfly).

$= 0$. However, including the *trans*-axial ligands lowers the dimer symmetry to C_{2h}, and due to the pyramidal coordination, the axis of each copper center is tilted with respect to the Cu_2O_2 plane and therefore the transfer matrix element $(h_{d\pi})_v$ is nonzero; its value was calculated from the relative, experimentally determined oscillator strengths of the π^*_σ and π^*_v absorption bands. Using the VBCI parameters given in Table 4, the A_g component of the π^*_σ −Cu(II) CT transition (electric dipole forbidden) was calculated to be approximately 2000 cm^{-1} above the electric dipole allowed B_u component (observed experimentally at 345 nm), and the splitting of the two components of the π^*_v−Cu(II) CT transition was calculated to be ∼3000 cm^{-1}, the CD-active band (A_g component) above the electric dipole allowed band (B_u component) in accord with experimental observations (Figure 9, left).

To apply the VBCI model to the C_{2v} butterfly core, values for Δ_σ, $(h_{d\pi})_\sigma$, Δ_v, and $(h_{d\pi})_v$ were determined. With the triplet ground state as a starting point (vide supra), transition state calculations (where half an electron is moved from a donor to an acceptor orbital and, after the potential is reconverged, the energy difference between the two orbitals is the electronic transition energy) were performed. The resulting energies can be related to the VBCI parameters using second-order perturbation theory, as given by the following equations (the left-hand side of the equations corresponds to the energies of the donor and acceptor orbitals from the transition state calculations):

$$E(\pi^*_v - \mathrm{HOMO}) = \Delta_v + ((h_{d\pi})_v^2/\Delta_v) + ((h_{d\pi})_\sigma^2/\Delta_\sigma)$$

$$E(\pi^*_v - \mathrm{LUMO}) = \Delta_v + 2((h_{d\pi})_v^2/\Delta_v) + ((h_{d\pi})_\sigma^2/\Delta_\sigma)$$

$$E(\pi^*_\sigma - \mathrm{HOMO}) = \Delta_\sigma + ((h_{d\pi})_v^2/\Delta_v) + ((h_{d\pi})_\sigma^2/\Delta_\sigma)$$

$$E(\pi^*_\sigma - \mathrm{LUMO}) = \Delta_\sigma + ((h_{d\pi})_v^2/\Delta_v) + 2((h_{d\pi})_\sigma^2/\Delta_\sigma) \quad (2)$$

Equations given in (2) were used to calculate the value of $(h_{d\pi})_v$, since the assumption (used for the C_{2h} model) that the HOMO−LUMO splitting is due to the interaction of the $d_{x^2-y^2}$ and π^*_σ orbitals only is no longer valid; the HOMO of the butterfly core contains approximately 20% peroxide π^*_v orbital. The energy of the DCT was calculated, starting from the triplet ground state, by transferring the two π^*_σ electrons into the HOMO and LUMO and summing the two transition energies. The MMCT zeroth-order energy was taken to be 6.5 eV, in accord with the planar structure. The calculated VBCI parameters for the butterfly core are given in Table 4.

It can be seen that the values for Δ_σ and $(h_{d\pi})_\sigma$ have decreased from those calculated for the planar C_{2h} model, reflecting the loss of interaction between the peroxide π^*_σ and the Cu $d_{x^2-y^2}$ orbitals of the butterfly core. In contrast, due to the greater interaction between the peroxide π^*_v and the Cu $d_{x^2-y^2}$ orbitals in the butterfly core, the magnitudes of the zeroth-order energy Δ_v and the transfer matrix element $(h_{d\pi})_v$ have increased compared with those for the planar core. Diagonalization of the secular determinants given in eqs 3 and 4, using the parameters given in Table 4, provides the energies for the π^*_σ and π^*_v CT states of the butterfly structure which are given in Table 4 and Figure 9 (right).

$$\begin{vmatrix} \langle {}^1A_1{}^{GS}\rangle - E & (h_{d\pi})_v & (h_{d\pi})_\sigma & 0 & 0 \\ (h_{d\pi})_v & \langle {}^1A_1{}^{CT}\rangle_v - E & 0 & (h_{d\pi})_v & 0 \\ (h_{d\pi})_\sigma & 0 & \langle {}^1A_1{}^{CT}\rangle_\sigma - E & (h_{d\pi})_\sigma & \sqrt{2}(h_{d\pi})_\sigma \\ 0 & (h_{d\pi})_v & (h_{d\pi})_\sigma & \langle {}^1A_1{}^{MMCT}\rangle - E & 0 \\ 0 & 0 & \sqrt{2}(h_{d\pi})_\sigma & 0 & \langle {}^1A_1{}^{DCT}\rangle - E \end{vmatrix} = 0 \quad (3)$$

$$\begin{vmatrix} \langle {}^1B_1{}^{CT}\rangle_v - E & 0 & (h_{d\pi})_v \\ 0 & \langle {}^1B_1{}^{CT}\rangle_\sigma - E & (h_{d\pi})_\sigma \\ (h_{d\pi})_v & (h_{d\pi})_\sigma & \langle {}^1B_1{}^{CT}\rangle_\sigma - E \end{vmatrix} = 0 \quad (4)$$

The A_1 component of the π^*_σ CT is calculated to be approximately 900 cm^{-1} *below* the B_1 component of the π^*_σ CT, in contrast to the results obtained for oxyhemocyanin[24] (C_{2h}), where the A_g component of the π^*_σ CT was calculated to be approximately 2000 cm^{-1} above the B_u component. The values of both Δ_σ and $(h_{d\pi})_\sigma$ have decreased due to the bending of the Cu_2O_2 core; therefore, both the A_1 and the B_1 components interact less strongly with the MMCT states compared with the planar model. More importantly, the A_1 component of the π^*_σ CT also does not interact as strongly with the A_1 ground state in the butterfly structure, allowing it to move below the B_1 component of the π^*_σ CT due to its additional interaction with the higher energy DCT (A_1 symmetry only). The absorption spectra obtained for the N*n* series all show the A_1 component of the π^*_σ CT (assigned using the TDVC model; vide supra) to lower energy than the B_1 component of the π^*_σ CT by 4000−7000 cm^{-1}.

The splitting between the two components of the π^*_v CT is calculated to be approximately 4000 cm^{-1}, compared with the splitting of ∼2900 cm^{-1} calculated for the planar C_{2h} core. This increased splitting has two contributions; due to the increased value of Δ_v and $(h_{d\pi})_v$, the B_1 component of the π^*_v CT is depressed more by its interaction with the MMCT state of the same symmetry and the A_1 component is repelled more strongly by its interaction with the ground state. The absorption spectra and resonance Raman profiles for the N*n* series show the splitting of the π^*_v states to be approximately 5000−6000 cm^{-1}, compared with the ∼3000 cm^{-1} splitting observed for oxyhemocyanin.

Thus, the VBCI model reproduces the lower energy A_1 component of the π^*_σ CT transition and the larger splitting of the two components of the π^*_v CT transition observed experimentally for the butterfly core. These effects are derived from the reduced interaction of the Cu $d_{x^2-y^2}$ orbitals and the peroxide π^*_σ orbitals and the significantly increased interaction of the Cu $d_{x^2-y^2}$ orbitals with the peroxide π^*_v orbitals, as also observed in the electronic structure calculations (vide supra).

Discussion

Resonance Raman and electronic absorption spectroscopy have identified the presence of four peroxide to copper(II) CT transitions in the complexes $[Cu_2(N\mathit{n}PY2)O_2]^{2+}$ (where n = 3−5): the two components of the in-plane peroxide π^*_σ−Cu(II) CT and the two components of the out-of plane peroxide π^*_v−Cu(II) CT transitions.

Using resonance Raman spectroscopy, it has been established that the additional band (not observed for planar Cu_2O_2 cores) in the 420−490 nm region of the absorption spectra of $[Cu_2(N\mathit{n}PY2)O_2]^{2+}$ is the second component of the π^*_σ−Cu(II) CT transition, which gains significant intensity upon bending the side-on peroxide-bridged dicopper core. For N5, where the Cu_2O_2 core is expected to be closer to planar, there is still reasonable intensity in the second component of the π^*_σ−Cu(II) CT transition due to the *cis*-axial ligand arrangement and the tilting of the copper axis with respect to the Cu_2O_2 plane. Absorption spectra very similar to those of $[Cu_2(N\mathit{n}PY2)(O_2)]^{2+}$ have been obtained for $[(TACN^iPr3)_2Cu_2O_2]^{2+}$ in acetone[10] and $[\{Cu(MePY2)\}_2O_2]^{2+}$ in dichloromethane;[26] resonance Raman spectra show that these solutions comprised of a mixture of side-on peroxide and bis(μ-oxo) cores, and the absorption band at ∼400 nm is associated with the bis(μ-oxo) isomer. Therefore, it is possible to obtain qualitatively similar absorption spectra from solutions of binuclear copper−oxygen complexes which have very different compositions. Indeed, in a recent study of the related system $[Cu^{II}(PY2CH_2CH_2CH_2Ph)(O_2)]^{2+}$ it was suggested that an absorption band at 430 nm may indicate the presence of the bis(μ-oxo) intermediate in solution; however, resonance Raman spectroscopy did not detect a peak characteristic of the bis(μ-oxo) core.[27] In light of the results presented here, it seems plausible that this band may be associated with a butterfly, side-on peroxide Cu_2O_2 core. Care should be exercised when proposing the nature of the reactive species present in solution on the basis of the analysis of absorption spectra only.

Electronic Structure and Spectroscopy. The electronic structure description obtained for the butterfly core from the Xα-SW calculations[16] differs from that of the planar Cu_2O_2 core in two main ways: the interaction between the peroxide π^*_σ orbitals with the Cu d orbitals decreases as the Cu_2O_2 is bent along the O−O axis, and the interaction between the peroxide π^*_v orbitals with the Cu d manifold increases.

The calculated differences in the electronic structures of the planar and butterfly cores are observed in the electronic absorption and resonance Raman spectra obtained for complexes exhibiting these two structural motifs. The intensity ratio of the high-energy component, B_1, of the π^*_σ−Cu(II) CT transition to the low-energy component, A_1, decreases and the total intensity of the two π^*_σ transitions decreases by 15% as the alkyl chain shortens. The changes observed in the relative intensities of the two components of the π^*_σ−Cu(II) CT are due to the change in overlap of the π^*_σ and Cu d orbitals upon bending the plane; as the core bends, the intensity of the higher energy $B_1(x)$ component of the π^*_σ−Cu(II) CT transition decreases as the "in-plane" overlap between the π^*_σ and Cu $d_{x^2-y^2}$ is reduced, and the intensity of the lower energy $A_1(z)$ component increases as the oxygens move out of the plane.

In contrast to the planar core, where the formally forbidden A_g component of the π^*_σ−Cu(II) CT is predicted to be above the B_{1u} component,[24] the A_1 component of the butterfly core is found below the B_1 component of the π^*_σ−Cu(II) CT. The energy gap between the B_1 and A_1 components increases with increased bending of the Cu_2O_2 core; the A_1 component moves to lower energy. From the application of the VBCI model, this trend is a direct result of the decreased overlap between the π^*_σ and Cu $d_{x^2-y^2}$ orbitals. The splitting of the two components of the π^*_v−Cu(II) CT observed in the N*n* series is larger than that observed in oxyhemocyanin. Again with the use of the VBCI model, this observation is reproduced and is a result of the increased interaction between the π^*_v and Cu $d_{x^2-y^2}$ orbitals.

The strength of the O−O bond increases as the alkyl chain linker shortens and the Cu_2O_2 core bends, as evidenced by the increased frequency of 25 cm^{-1} (from 740 to 765 cm^{-1}) of the peroxide O−O stretch on going from N5 to N3. Consistent with this trend, a resonance Raman spectrum obtained for the related complex $[\{Cu(MePY2)\}_2(O_2)]^{2+}$, where the alkyl chain linker is replaced with methyl groups at the amino nitrogens, has a peroxide O−O stretch at 730 cm^{-1}.[26,28] The Cu_2O_2 core in $[\{Cu(MePY2)\}_2(O_2)]^{2+}$ is expected to be planar, since the linker which constrains the Cu−Cu distance and causes the butterfly distortion in N3, N4, and N5 has been removed.

The low frequency observed for the peroxide O−O stretch in side-on peroxide-bridged dicopper cores has been proposed to be due to the small amount of σ^* present in the HOMO.[22] Donation into this strongly O−O antibonding orbital leads to a weak O−O stretch. The shift observed in the frequency of the O−O stretch for N5, N4, and N3 may be expected to be the result of a change in the occupancy of the σ^* orbital. However, the Xα calculations show that the populations of both the σ^b and σ^* atomic orbitals do not change upon bending the core at the O−O axis, consistent with the cylindrical symmetry of σ^* along the O−O axis. Rather, the small increase in the strength of the O−O bond observed upon bending the Cu_2O_2 core is mainly due to a symmetry-allowed interaction between the peroxide π^*_v orbital and the Cu $4p_y$ orbital, which leads to a depopulation of the π^*_v orbital.

Reactivity. It has been suggested[29] that the peroxide intermediate P in methane monooxygenase could have a butterfly structure and that this moiety is a precursor to Q, the bis(μ-oxo) intermediate. These studies on the N*n* series show that the peroxide O−O bond becomes stronger upon bending the Cu_2O_2 plane. The σ^* orbital, which is populated to a substantial degree in the bis(μ-oxo) core, is only ∼6% occupied in the butterfly core, very similar to the planar side-on peroxide core. The peroxide valence orbitals are overall less populated in the butterfly structure, and hence, the calculated charge on the peroxide oxygens has decreased when compared with the planar

(26) Obias, H. V.; Lin, Y.; Murthy, N. N.; Pidcock, E.; Solomon, E. I.; Ralle, M.; Blackburn, N.; Neuhold, Y.-M.; Zuberbühler, A. D.; Karlin, K. D. Submitted for publication.

(27) Itoh, S.; Nakao, H.; Berreau, L. M.; Kondo, T.; Komatsu, M.; Fukuzumi, S. *J. Am. Chem. Soc.* **1998**, *120*, 2890−2899.

(28) Resonance Raman spectra obtained for solutions of N4 in acetone at concentrations of >8 mM, oxygenated by passing O_2 over the surface of the solution at −80 °C, have a peak at 730 cm^{-1}, which gains intensity with time. It is assigned as an intermolecular peroxide stretch[14] where O_2^{2-} is bridging between the copper atoms of two $[Cu_2(N4PY2)]^{2+}$ units.

(29) Liu, K. E.; Valentine, A. M.; Wang, D.; Huynh, B. H.; Edmondson, D. E.; Salifoglou, A.; Lippard, S. J. *J. Am. Chem. Soc.* **1995**, *117*, 10174−10185.

Cu_2O_2 core. Therefore, a butterfly distortion of the core does not lower the energy of the reaction pathway to a bis(μ-oxo) core and the bridging peroxide of a butterfly core can be described as less electron-rich than the planar side-on bridged peroxide, and certainly less "oxide-like".

Frontier molecular orbital theory, which has been used to examine the reactivity of the planar side-on peroxide and bis-(μ-oxo) cores toward electrophilic aromatic substitution reactions, can be extended to the butterfly core.[14] The important frontier molecular orbitals in electrophilic aromatic substitution are the LUMO of the electrophile and the HOMO of the nucleophile: i.e. the LUMO of the Cu_2O_2 core and the HOMO of the arene ring. The symmetry of the interacting orbitals and the amount of relevant atomic orbital present in the frontier molecular orbitals has to be considered; a small HOMO−LUMO splitting will yield a large interaction energy.

The relative reactivities of the butterfly and planar side-on peroxide-bridged binuclear copper cores with respect to electrophilic aromatic substitution can be compared using benzene as the nucleophile; its HOMO is at −9.2 eV, estimated from the first ionization potential. In the planar Cu_2O_2 core the LUMO ($LUMO_{planar}$) consists of the Cu $d_{x^2-y^2}$ orbital and 15% peroxide π^*_σ orbital and is found at −5.4 eV. The LUMO of the butterfly core ($LUMO_{butterfly}$) is found at −4.3 eV and consists of, like the planar Cu_2O_2 core, Cu $d_{x^2-y^2}$ and 15% peroxide π^*_σ. The increased $HOMO_{benzene}$−$LUMO_{butterfly}$ splitting indicates the butterfly Cu_2O_2-containing complexes will be slightly less reactive with nucleophiles with low-lying HOMOs (i.e. benzene) than with complexes containing the planar side-on peroxide core.

Similarly, FMO theory can be applied to hydrogen atom abstraction reactions. The unoccupied molecular orbital of the Cu_2O_2 core ("electrophile") that will participate in H atom abstraction reactions is likely to contain σ^*, since it will have good overlap with the σ-character orbitals of the occupied C−H molecular orbital of the "nucleophile", found to deeper binding energy ($\leq$8 eV).[30] In both planar and butterfly structures the σ^*-containing, unoccupied MO is to high energy (ca. −1 eV), indicating that H atom abstraction is not a particularly favorable reaction for the side-on bridged peroxide cores. The percentage of σ^* present in the lowest energy unoccupied σ^*-containing MO in the butterfly structure is only 35%, compared to the 60% present in the planar Cu_2O_2 core, further disfavoring H atom abstraction for a bent Cu_2O_2 core. The reactivity of the butterfly cores with respect to H-atom abstraction is currently under investigation.[31]

In summary, the electronic structure of a side-on peroxide-bridged dicopper core containing a butterfly structural moiety has now been defined. The changes in electronic structure have been correlated with trends observed in the intensity and position of bands in the absorption spectra and in O−O stretching frequencies in the resonance Raman spectra for the $[Cu_2(N\mathit{n}PY2)(O_2)]^{2+}$ series. The application of frontier molecular orbital theory to compare the relative reactivities of the planar and butterfly $[Cu_2(\mu\text{-}\eta^2\text{:}\eta^2)(O_2)]^{2+}$ cores suggests that the butterfly core is slightly less reactive with respect to electrophilic substitution and H atom abstraction reactions.

Acknowledgment. We thank Dr. Frank Neese for helpful discussions. This work was supported by grants from the National Institutes of Health (Grant Nos. DK31450 (E.I.S.) and GM28962 (K.D.K.)).

Supporting Information Available: Tables giving coordinates used in SCF-Xα calculations of a butterfly and a planar $[(NH_3)_4Cu_2(O_2)]^{2+}$ core and intensity vs energy profiles of $[Cu_2(N3PY2)O_2]^{2+}$ and $[Cu_2(N5PY2)O_2]^{2+}$ (PDF). This material is available free of charge via the Internet at http://pubs.acs.org.

JA983310E

(30) I. Fleming. *Frontier Orbitals and Organic Chemical Reactions*; Wiley: Chichester, U.K., 1996.
(31) Liang, H.-C.; Karlin, K. D. Unpublished results.
(32) Lever, A. B. P. *Inorganic Electronic Spectroscopy*; Elsevier: Amsterdam, 1968.